Stokes shift spectroscopy pilot study for cancerous and normal prostate tissues

J. Ebenezar,[1] Yang Pu,[2] W. B. Wang,[2] C. H. Liu,[2] and R. R. Alfano[2,*]

[1]PG & Research Department of Physics, Jamal Mohamed College, Tiruchirappalli, Tamilnadu 620020, India

[2]Institute for Ultrafast Spectroscopy and Lasers, Department of Physics, The City College of New York,
160 Convent Avenue, New York, New York 10031, USA

*Corresponding author: ralfano@sci.ccny.cuny.edu

Stokes shift spectroscopy (S3) is an emerging approach toward cancer detection. The goal of this paper is to evaluate the diagnostic potential of the S3 technique for the detection and characterization of normal and cancerous prostate tissues. Pairs of cancerous and normal prostate tissue samples were taken from each of eight patients. Stokes shift spectra were measured by simultaneously scanning both the excitation and emission wavelengths while keeping a fixed wavelength interval $\Delta\lambda = 20$ nm between them. The salient features of this technique are the highly resolved emission peaks and significant spectral differences between the normal and cancerous prostate tissues, as observed in the wavelength region of 250 to 600 nm. The Stokes shift spectra of cancerous and normal prostate tissues revealed distinct peaks around 300, 345, 440, and 510 nm, which are attributed to tryptophan, collagen, NADH, and flavin, respectively. To quantify the spectral differences between the normal and cancerous prostate tissues, two spectral ratios were computed. The findings revealed that both ratio parameters $R_1 = I_{297}/I_{345}$ and $R_2 = I_{307}/I_{345}$ were excellent diagnostic ratio parameters giving 100% specificity and 100% sensitivity for distinguishing cancerous tissue from the normal tissue. Our results demonstrate that S3 is a sensitive and specific technique for detecting cancerous prostate tissue. © 2012 Optical Society of America

OCIS codes: 170.6280, 300.6170.

1. Introduction

Prostate cancer is the second leading cause of cancer death among American men. During 2010, an estimated 217,730 new prostate cancer cases were reported in the United States, and it was predicted that among them, 32,050 men might die [1]. Currently, prostate cancer diagnosis is based on a prostate specific antigen (PSA) test and digital rectal examination (DRE). If either of these two tests is abnormal, a biopsy is usually performed guided by transrectal ultrasound (TRUS). Although a TRUS-guided biopsy is considered the gold standard, it suffers from lack of sensitivity and specificity and leads to a significant number of false negatives, which then often leads to unnecessary biopsies, patient trauma, and the time needed to obtain a histopathological diagnosis [2]. Consequently, new detection technologies are needed that can overcome the current limitations and improve patient well-being.

Optical spectroscopy offers a novel diagnostic approach for tissue and can be considered as an alternative technique to conventional methods because of its advantages, such as minimal invasiveness, less time, and reproducibility. For more than three decades, various optical spectroscopic techniques for cancer diagnosis have been widely explored as potential diagnostic tools in the discrimination of normal from abnormal tissues. In the 1980s, Alfano's group first reported on the light-induced fluorescence differences from malignant and nonmalignant breast and lung tissues [3]. Since then, some groups around the world have reported the use of native fluorescence

spectroscopy [4,5] and/or diffuse reflectance spectroscopy [6,7] for diagnosis of cancers in different organs. These reported studies indicate that optical spectroscopy has the potential to improve the screening and early detection of cancer. The optical spectra method, known as "optical biopsy," as termed by Alfano, is a potential technique by which the medical community can diagnose tissues without removing them.

Native fluorescence of tissues, also called autofluorescence, is believed to be produced by several endogenous fluorophores, such as tryptophan, collagen, elastin, a reduced form of nicotinamide adenine dinucleotide (NADH), flavin adenine dinucleotide (FAD), and endogenous porphyrins. During the development from benign prostatic hyperplasia to premalignant (dysplastic) and malignant stages, prostate cells undergo proliferations that modify these fluorophore levels [8]. Additionally, the connective tissue frameworks of prostate tissue can be impaired during cancer development [9]. Such changes are likely to alter both tissue morphology and biochemistry, which could be detected using tissue fluorescence spectroscopy [10]. Thus, by measuring the fluorescence signal from tissue, changes in tissue structure and composition and information concerning the pathological state of the tissue could be obtained [11,12].

Cells/tissues contain several key fluorophores with broad and partly overlapped excitation and emission spectra [13]. Further, each fluorophore has a distinct absorption peak wavelength and a characteristic "fingerprint" peak emission wavelength [14]. The emission spectra at one or more excitation wavelengths or excitation spectra corresponding to one or more emission wavelengths have been used for diagnostic purposes [15]. The conventional laser-induced fluorescence spectroscopic method for cancer detection has limited applicability since most tissue fluorescence spectra have a series of overlapping bands from different fluorophores, and it often cannot be resolved satisfactorily by a single-excitation wavelength. To overcome this problem, multiple-excitation wavelengths are sequentially used to generate an excitation-emission matrix (EEM) in order to identify the optimal excitation wavelengths at which tissue classification is enhanced and to determine the origin of the measured fluorescence signal in a more reliable manner [5]. However, EEM measurement requires a large number of fluorescence emission scans at sequential excitation wavelengths at small wavelength intervals, and this is time-consuming. In order to reduce time consumption, a two-dimensional detector, such as a CCD camera, is used in conjunction with a spectrograph.

Alfano and Yang were the first to introduce the physical concept of Stokes shift spectroscopy (S3) as a rapid method for diagnosing diseased tissue that depends on both absorption and emission properties of the fluorophores [16]. In S3, the excitation wavelength λ_{ex} and the emission wavelength λ_{em} are scanned synchronously with a constant wavelength interval $\Delta\lambda = \lambda_{em} - \lambda_{ex}$ between the excitation and emission. Earlier, this technique was called synchronous fluorescence spectroscopy, and it begins with a multicomponent analysis to obtain spectral emission peaks of tissue samples, and it enhances the selectivity in the assay of complex systems [17]. Recently, S3 was used as a potential tool for the diagnostic purposes. Ebenezar *et al.* investigated the potential use of S3 as a diagnostic tool for the discrimination between normal and abnormal cervical and breast tissues [18,19]. Masilamani *et al.* studied the use of S3 in the discrimination of benign and malignant prostate tissues [20]. However, to the best of our knowledge, no report is available using S3 technique for the comparison and discrimination of cancerous and normal prostate tissues from the same patients. Therefore, this paper is designed to demonstrate the potential use of the S3 technique to detect and characterize the normal and cancerous prostate tissues from the same patients, and to determine the optimal offset wavelength $\Delta\lambda$ for distinguishing cancerous tissue from normal prostate tissue.

2. Materials and Methods

A. Tissue Samples

A total of sixteen fresh human prostate tissue samples were collected from eight patients from the Cooperation Human Tissue Network (CHTN) under the Institutional Review Board approval of The City College of New York. Each patient provided a pair of normal and cancerous samples. The spectroscopic data were classified into two groups: (1) normal and (2) cancerous tissues according to their post-spectroscopy studies. The optical biopsy of each tissue sample was compared to the histopathology analyses.

B. S3 Measurements

The Stokes shift (SS) spectra of *ex vivo* prostate tissues were recorded using spectrofluorometer (LS 50, PerkinElmer). The prostate tissue samples of solid chunks of approximately 1.5 mm × 1 mm × 0.3 mm (length × width × thickness) were placed in a quartz cuvette with the epithelium toward the face of the cuvette and the beam. The excitation light of approximately 2 mm × 4 mm was incident perpendicular to the face of the tissue epithelium surface, and the emitted fluorescence light was collected at a 90° angle to the excitation light. During data acquisition, the excitation and emission monochromators had fixed band passes of 3 nm each, and the wavelength increment was set at 0.5 nm. The variation in the excitation light source intensity as a function of wavelength was taken into account during SS spectra measurements. This was done by detecting the fluorescence signal (S) by the photomultiplier tube as well as recording the reference excitation intensity (R) by a photodiode and taking their ratio S/R to serve as the final S3 signal to account for the wavelength-dependent light intensity.

C. Optimization of Offset Wavelength $\Delta\lambda$

The SS is dependent upon the vibrational and electronic interaction and the polarity of the host environment surrounding the emitting organic molecules. The wavelength interval of the SS spectrum can be simply compressed or expanded just by decreasing or increasing the selected $\Delta\lambda$ parameter [19]. During S3 acquisition, the excitation and emission monochromators were scanned simultaneously at the same speed with a constant wavelength interval $\Delta\lambda$ between them. In this paper, we investigated various $\Delta\lambda$ values, ranging from 10 to 50 nm, in increments of 10 nm. Among the five $\Delta\lambda$ alues, a $\Delta\lambda = 20$ nm revealed four key identifiable fluorophores with a good signal-to-noise ratio. Therefore, the value of $\Delta\lambda = 20$ nm was selected as the favored offset wavelength interval for the entire series of investigation. The S3 of normal and cancerous prostate tissues were recorded in wavelengths of 250 to 600 nm, where $\Delta\lambda = 20$ nm, and with a scanning speed of 5 nm/sec. Because the S3 measurements involved the simultaneous scanning of both excitation and emission monochromators, significant contribution from the excitation light source was expected. By dividing each of the SS spectra by the lamp spectrum measured under the same instrumental parameters, the contribution from the excitation light source to the SS spectra was counted.

D. Statistical Analysis

The measured spectral data were analyzed statistically to discriminate cancerous tissue from normal prostate tissue. Data were initially preprocessed by normalizing each spectral profile with respect to the maximum fluorescence intensity of spectrum. From the normalized spectrum, two intensity ratios were calculated at different wavelengths corresponding to the characteristic spectral features of different groups of the prostate tissues studied. The mean and standard deviation values were calculated for each group of prostate tissue, and their statistical significance was verified using an unpaired Student's t-test to calculate the level of physical significance p with 95% confidence interval using origin statistical software (OriginPro7). The corresponding tissues, which yielded significant differences ($p < 0.005$) in the ratio values, were selected for further histopathological analyses.

The classification analysis was determined on the basis of discrimination cutoff values. Discrimination cutoff lines are drawn between the normal (mean of all normal tissues) and cancerous (mean of all cancer tissues), at values that correspond to the mean ratio value of the respective groups. The sensitivity and specificity in discriminating each of these categories were determined on the basis of the cutoff values identified by ratio method by validation with the gold standard, namely, histopathological results of biopsy specimens taken from SS emission measurement sites. Similar ratio intensity variable methods have been adopted by earlier researchers to discriminate

normal from different tissue categories of bladder tissues, and the sensitivity and specificity were determined on the basis of the discrimination cutoff lines [5].

3. Results

The normalized mean S3 of cancerous (solid) and normal (dash) prostate tissues in the wavelength region between 250 and 600 nm is shown in Fig. 1. The normal tissues show a small hump around of 307 nm, with a single primary band centered at 345 nm, a small shoulder around 375 nm, and secondary peaks observed at 405, 440 and 510 nm. Although cancerous tissue is found to exhibit two primary, highly resolved bands at 297 and 345 nm, with secondary peaks observed at 440 and 510 nm, and the spectral band at 297 nm was higher than that at 345 nm. From this normalized spectrum, it was also observed that all the spectral bands are highly resolved, and one could discern the spectral shift of primary emission bands between normal and cancerous tissues. For example, the normalized spectra of normal tissues show an emission band at 307 nm, which was blueshifted to 297 nm for cancerous tissues. In addition, a spectral dip or valley was also observed around 425 nm for normal and cancerous tissues. It was noted that the valley at 425 nm is deeper in the case of cancerous than normal tissues.

A. S3 Measurements of Standard Fluorophores

To investigate the origin of the observed spectral peaks from normal and cancerous prostate tissues and to assign them to various endogenous fluorophores, the S3 of commercially obtained fluorophores (Sigma Chemicals, USA) of tryptophan, collagen, NADH, and FAD were measured with the same experimental parameters maintained as for the prostate tissues. The SS spectra of the commercial-grade fluorophores were corrected for the variation in the lamp intensity and normalized with respect to the corresponding peak intensity. Figure 2 shows the normalized SS spectra of the standard
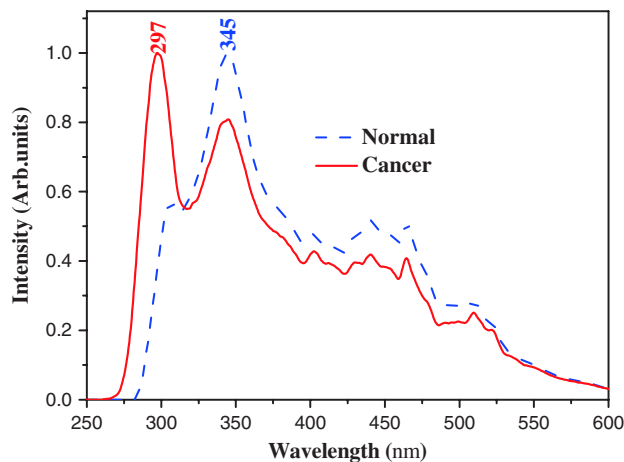

Fig. 1. (Color online) Normalized mean Stokes shift spectra of cancerous (solid) and normal (dash) prostate tissues.
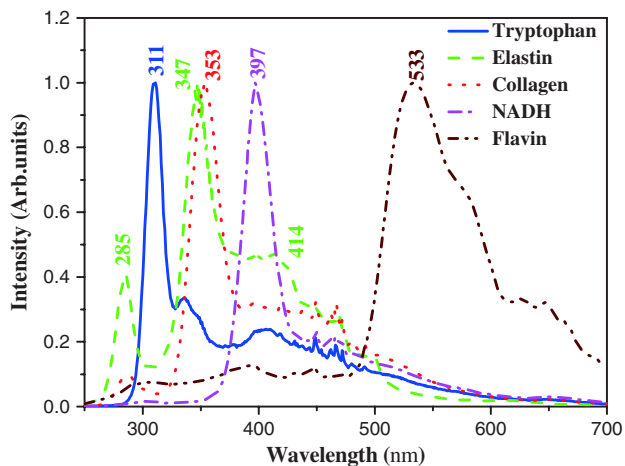
Fig. 2. (Color online) Normalized Stokes shift spectra of standard fluorophores of tryptophan (solid), elastin (dash), collagen (dot), NADH (dash dot), and FAD (dash dot dot).

Fig. 3. Scatter plot of intensity ratio of I_{297}/I_{345} for normal (•) and cancerous (■) prostate tissues.

fluorophores, such as tryptophan (solid), elastin (dash), collagen (dot), NADH (dash dot) and FAD (dash dot dot), with their narrow emission peaks observed at 311, 347, 353, 397, and 533 nm, respectively. The SS spectra of elastin also showed secondary peaks at 285 nm, with a small shoulder around 414 nm. Further, the fine structures observed in the wavelength region between 440 and 500 nm may be due to the stray light contribution from the xenon lamp passing through the exit slit of the excitation monochromator. A sharp spectral feature was observed at 467 nm due to the contribution from the xenon lamp source.

B. Results of Statistical Analysis

In order to validate the diagnostic utility of the observed spectral signatures between normal and cancerous tissues, two ratio variables were introduced for SS spectra, with $\Delta\lambda = 20$ nm. The mean and standard deviation of the SS spectral ratios of normal and cancerous prostate tissues were calculated, and the results are listed in Table 1 along with p values. The statistical significance was computed through an unpaired Student's t-test to determine the level of significance p. The p values for both the ratio variables are less than 0.005, indicating a high statistical significance. From Table 1, for both ratio variables $R_1 = I_{297}/I_{345}$ and $R_2 = I_{307}/I_{345}$, the mean value of the normal tissue was lower than that of the cancerous tissue. In the SS spectrum, it is the relative intensities between the maxima that are of importance rather than the numerical intensity
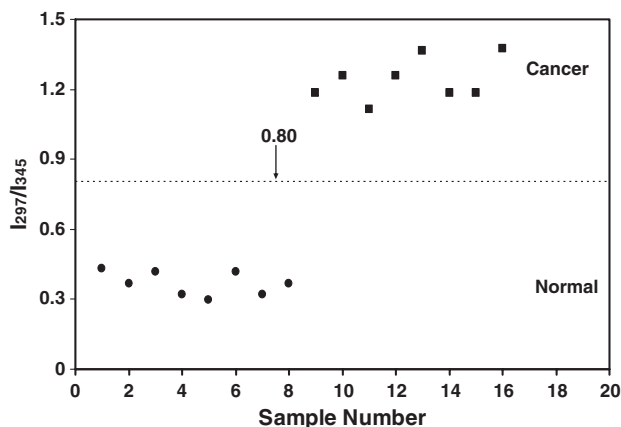
value of each maximum. Table 1 shows the computed ratios of the fluorescence peak intensities at 297 to 345 nm (R_1), and 307 to 345 nm (R_2), correlating with their histologic findings. For example, the mean ratio value of R_1 in normal tissues was 0.36 ± 0.05, which is significantly different from the mean value of 1.24 ± 0.09 in cancerous tissues (unpaired Student's t-test, $p < 0.005$). By selecting the I_{297}/I_{345} of ~0.80 as the demarcation ratio level (between the normal and cancerous tissues), it is found to yield 100% specificity and 100% sensitivity for differentiating cancerous from normal tissues (Fig. 3). Similarly, the mean ratio value of R_2 for normal tissue was 0.57 ± 0.05, which is also significantly different from the mean value of 0.92 ± 0.05 for cancerous prostate tissues (unpaired Student's t-test, $p < 0.005$). By selecting I_{307}/I_{345} of ~0.74 as a cutoff for tissue demarcation, 100% specificity and 100% sensitivity were achieved (Fig. 4).

4. Discussion

The potential use of the S3 technique in detection and characterization of normal and cancerous prostate tissues was explored, and the spectral data were analyzed by a simple statistical method, which validated the diagnostic potentiality of the present method. The comparison of S3 spectra of normal and cancerous tissues with those corresponding to commercial-grade standard fluorophores suggests that the peaks observed around 297, 307, 345, 440, and 510 nm may be primarily attributed to tryptophan, collagen and/or elastin, NADH, and FAD, respectively. Similar peaks of S3 were reported earlier in the discrimination of normal and different

Table 1. Mean ±SD of the Stokes Shift Spectral Ratios of Normal and Cancerous Prostate Tissues

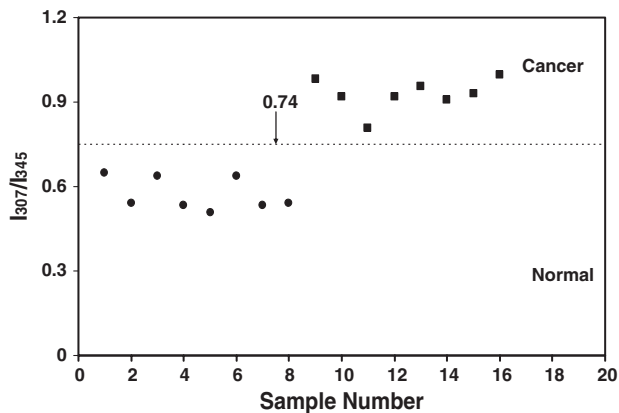| Tissue types	Spectral Intensity			Intensity ratio $R_1 = I_{297}/I_{345}$	Intensity ratio $R_2 = I_{307}/I_{345}$
	At 297 nm	At 307 nm	At 345 nm		
Normal	0.36 ± 0.05	0.57 ± 0.05	0.99 ± 0.00	0.36 ± 0.05	0.57 ± 0.05
Cancerous	0.98 ± 0.01	0.73 ± 0.03	0.79 ± 0.05	1.24 ± 0.09	0.92 ± 0.05
P value	<0.005	<0.005	<0.005	<0.005	<0.005

Fig. 4. Scatter plot of intensity ratio of I_{307}/I_{345} for normal (•) and cancerous (■) prostate tissues.

pathological studies of cervical tissues [18]. In this paper, the wavelengths of the spectral peaks observed for prostate tissues were not exactly the same as those of the standard fluorophores. This observed spectral shift of the peak positions in the spectra of prostate tissues may be due to the different microenvironments of these endogenous fluorophores in tissues. In particular, the band position of standard fluorophore of NADH at 397 nm does not exactly match our prostate tissue band position, which has been observed around 440 nm. Earlier reported studies have shown that exact determination of NADH emission is difficult because this compound significantly changes the spectral shape and intensity after undergoing oxidation after resection [13]. In addition, the fluorescence data of NADH compound obtained from *ex vivo* tissue may not accurately represent the *in vivo* or living situation [21]. Thus oxidation of tissue fluorophores will influence the fluorescence properties of the tissues, which leads to change in spectral peak positions and the line width and fluorescence intensities [22,23].

Distinct salient differences in the spectral signatures of tryptophan, collagen and/or elastin, NADH, and FAD were observed from normal and different pathological conditions of prostate tissues, as shown in Fig. 1. The normal tissue exhibits a small peak around 307 nm, most likely due to tryptophan, an aromatic amino acid. This peak was significantly higher, and it shifted to 297 nm for cancerous tissues. Table 1 also shows that the intensity of the tryptophan emission band was higher in the cancerous tissues (0.98 ± 0.01 at 297 nm and 0.73 ± 0.03 at 307 nm) than in normal tissues (0.36 ± 0.05 at 297 nm and 0.57 ± 0.05 and 307 nm). Significantly, the tryptophan emission band was lower (0.57 ± 0.05 at 307 nm) for normal tissues, and it was noticed that the same band was blueshifted with increased emission intensity (0.98 ± 0.01 at 307 nm) for cancerous tissues. The striking observation is the increase in the tryptophan fluorescence signals in cancerous tissues relative to its normal counterpart. This increase is probably due to hyperactivity or epithelium

glandular proliferation resulting in higher transient concentration of proteins in cells and/or increased thickness of the epithelium [9,24]. The observed increase in tryptophan fluorescence correlates with the earlier reported data on cervical epithelial cancer cells, non-melanoma, and bladder cancerous tissues [4,5,25]. In addition to the increase in tryptophan fluorescence intensity, the peak emission wavelength was blueshifted to 297 nm for cancerous tissues in comparison with the normal tissues. This observed blueshift may be attributed to changes in the local microenvironment and conformational changes of the protein-bound tryptophan, relative to the free amino acid [26]. Similar spectral blueshifts have been noted in human laryngeal epithelial cells [27], carcinogen-transformed human bronchial epithelial cells [28], and SS spectra of breast tissues [19]. Further, it is suggested that sensitivity of tryptophan fluorescence and its peak emission due to polarity and mobility of environment makes tryptophan fluorescence useful for monitoring structural changes in a protein [29]. Based on the results, it is concluded that changes in intrinsic tryptophan fluorescence and its peak emission wavelength from cancerous prostate tissues can be used as one of the diagnostic criteria for classifying early neoplastic changes.

The structural proteins collagen and/or elastin have been noted in the S3 spectrum. As we know, collagen and/or elastin is a major component of extracellular matrix and dominates the stroma fluorescence associated with crosslinks. From Fig. 1, the primary prominent band was observed for the normal tissue at 345 nm, corresponding to structural protein collagen and/or elastin, with a small shoulder around 375 nm, and secondary peak was observed at 405 nm due to elastin. These bands are drastically decreased in the cases of cancerous prostate tissues. Table 1 also shows that the intensity of collagen emission band (0.99 ± 0.00 at 345 nm) was high in normal tissues and low (0.79 ± 0.05 at 345 nm) in cancerous tissues. In normal prostate tissues, the collagen and elastin network is dense, with larger numbers of fibers compared to non-uniform of size and shape of the epithelial cells, and loss and disintegration of collagen and elastin fibers in the cancerous prostate tissue was expected [24,30,31]. The significant decrease of collagen and/or elastin fluorescence in cancerous prostate tissues may be due to structural changes in the epithelium, and sub-epithelial collagen network may be due to nuclear enlargement and because epithelial cells are crowded with increased cell density, loss of cellular maturation, and overall thickening of the epithelium [8,10,32]. Thus, increased thickness of the epithelium in malignant prostate glands attenuates both excitation light and emission fluorescence light from the vascular stroma, leading to reduced penetration depth of the excitation light as well as the re-absorption of the emitted fluorescence. This may present a potential criterion for prostate cancer detection. This criterion agreement with reported studies has shown that collagen

fluorescence is decreased in cancerous prostate tissues [8].

The characteristic hemoglobin absorption features were clearly found as a dip at 420 nm for normal and cancerous prostate tissues. The hemoglobin absorption is deeper in the case of cancerous tissues than for normal tissues due to possible increase of hemoglobin content from angiogenesis [32]. Most cancerous tissue is known to exhibit increased vasculature due to angiogenic developments with recurrence in hypoxia, and, hence, there is increased blood content in superficial tissue layers, which leads to increased hemoglobin absorption when compared to normal tissues [33]. This hypothesis is also consistent with the findings of earlier reports on S3 of cervical [18] and breast tissues [19] and other studies by Demos et al. [14] and Volynskaya et al. [34].

In addition to this, in Fig. 1, the normal tissue exhibits a broad peak around 440 nm and has a small sharp peak at 510 nm at a longer wavelength. However, cancerous prostate tissues also reveal similar spectral bands but with a less fluorescence intensity compared with the normal tissues. The observed spectral bands at 440 and 510 nm may be attributed to the coenzyme of NADH and FAD. The relative decrease of NADH and FAD fluorescence in malignant prostate tissues may be due to changes in tissue morphology (thickening of epithelium), the decrease of fluorophores (NADH and FAD) quantum yields, and/or oxidation of tissue fluorophores [5,22].

The present result shows that the overall S3 signature provides information about tissue architecture (epithelial thickness), changes in absorption due to hemoglobin, and concentration of fluorescing molecules, which can be correlated to histological changes. Therefore, alteration in tissue architecture that inhibits excitation photons from reaching the native fluorophores and/or the emission photons from the fluorophores from escaping from the tissue could be detected by the S3. Additionally, as the hemoglobin concentration increased, the fluorescence intensity decreased and the fluorescence profile was altered significantly. Thus, changes in the concentration of the key native fluorophores could alter the emitted fluorescence in a single scan, which is manifested in our study.

Many studies have been reported that the fluorescence spectral intensity ratio could be used as a potential tool for tissue diagnosis [5,18–20]. In this paper, a simple classification method was adopted based on the ratio values estimated from the intensities at different wavelengths characterizing the peaks of different groups under study. To quantify the observed spectral results and to estimate the diagnostic potentiality of the present technique, two intensity ratios, such as I_{297}/I_{345} for normal tissues and I_{307}/I_{345} for cancerous tissues, were selected. Each emission wavelength used in these ratios represents a specific fingerprint of one fluorophore. The component identified as I_{307} represents the peak emission wavelength of tryptophan for normal tis-

sues, whereas I_{207} represents the peak emission wavelength of tryptophan for cancerous tissues, and I_{345} represents the peak emission wavelength of collagen and/or elastin from normal and cancerous tissues. Both intensity ratio values increase significantly for cancerous tissues in comparison with normal tissues. From these ratio parameters, we found variations in the relative distribution of tryptophan, collagen and/or elastin corresponding to the different histopathology of the tissues.

In this paper, we performed the classification analysis for two ratio parameters (I_{297}/I_{345} and I_{307}/I_{345}) in order to find out the specificity and sensitivity of the present technique to discriminate between two groups. Figure 3 shows the scatter plot of the spectral intensity ratio of I_{297}/I_{345} from sixteen samples from eight patients categorized as normal prostate tissues ($n = 8$) and cancerous prostate tissues ($n = 8$). The classification specificity and sensitivity in discriminating each of these categories were determined on the basis of discrimination cutoff values, given in the scatter plot (Fig. 3). For example, the cutoff line discriminating the normal from the cancerous were drawn at 0.80, corresponding to the mean ratio of normal (0.36) and the mean of the cancerous (1.24) group. For the I_{297}/I_{345} ratio, by selecting a cutoff at the mean (0.80) of the normal and cancerous tissues yield, 100% specificity and 100% sensitivity was obtained for discrimination of the normal from the cancerous. Similarly, we performed other ratio parameter I_{307}/I_{345} for the same classification analysis. Figure 4 shows the scatter plot of the spectral intensity I_{307}/I_{345} ratio, the cutoff line drawn at 0.74 discriminates the normal from cancerous, with the specificity and sensitivity of 100% and 100%, respectively.

Statistical analysis showed that both intensity ratios yielded 100% diagnostic sensitivity and specificity. Since the increased value of the fluorescence ratios of I_{297}/I_{345} and I_{307}/I_{345} for cancerous prostate tissues compared to normal tissue reflects an increase in the tryptophan fluorescence contribution and a decrease in the collagen and/or elastin fluorescence contribution. Among the all the fluorophores, the finding of increased band of tryptophan fluorescence and decreased fluorescence of collagen and/or elastin band from prostate cancer could be particularly useful for detecting prostate cancer.

The major advantage of the S3 technique is that all the fluorophores in complex structures, such as tissue, are excited under optimal conditions, such as wavelength of excitation, slit widths, scan speed, and scan range, which is practically impossible in the case of conventional fluorescence measurements. In the case of conventional fluorescence measurements, optimal conditions are chosen based on the fluorophores of interest. Though, EEM offers great resolution, it takes some time to carry out, even with multichannel detectors. Also, the large amount of data of EEM could significantly slow down the data processing procedures and clearly is impractical in a

clinical setting. On the other hand, S3 represents the diagonal scan over the entire EEM, thereby reducing the time of data acquisition without any alterations in the details over the entire spectral range of the different fluorophores present in the different tissues. The S3 technique reduces the time of data acquisition and can be identified in a specific spectral range with narrower spectral band attributed by each fluorophore than the conventional fluorescence spectrum. S3 improves the diagnostic capability of optical spectroscopy for prostate cancer diagnosis because all the key fluorophores, such as tryptophan, collagen and/or elastin, hemoglobin (absorption), NADH, and FAD, can be obtained in a single scan [16], and they are reported as cancer markers [8–11]. On the basis of above factors, S3 may also be considered as a technique that is alternative or/and complementary to the existing conventional methods for tissue diagnosis.

5. Conclusion

This paper suggests that S3 holds the potential for differentiating between diseased and normal prostate tissues *in vitro*. Results of the current study demonstrate that spectral changes due to the changes of contents of tryptophan, collagen and/or elastin, NADH, and FAD have good diagnostic potential. Two ratio parameters ($R_1 = I_{297}/I_{345}$ and $R_2 = I_{307}/I_{345}$) were empirically selected and evaluated by an unpaired Student's t-test, which showed useful diagnostic information with excellent discrimination of mean ratio values between normal and cancerous prostate groups. To improve on the diagnostic capability of S3, a larger number of samples of normal and different pathological prostate tissues would need to be validated in blinded manner. Such investigations with a large group of tissue biopsies will be useful for the development of a statistical database and a user-friendly diagnostic algorithm that could facilitate a real-time *in vivo* clinical diagnosis of prostate cancer. Currently, we are working on the above aspects to prove S3 as a useful and novel technique in the diagnostic clinical oncology for different tissue types.

References

1. American Cancer Society, Cancer Facts and Figures (American Cancer Society, 2009).
2. L. V. Rodriguez and M. K. Terris, "Risks and complications of transrectal ultrasound guided prostate needle biopsy: a prospective study and review of the literature," J. Urol. **160**, 2115–2120 (1998).
3. R. R. Alfano, D. Tata, J. Cordero, P. Tomashefsky, F. Longo, and M. Alfano, "Laser-induced fluorescence spectroscopy from native cancerous and normal tissue," IEEE J. Quantum Electron. **20**, 1507–1511 (1984).
4. R. R. Alfano, G. C. Tang, A. Pradhan, W. Lam, D. J. Choy, and E. Opher, "Fluorescence spectra from cancerous and normal human breast and lung tissues," IEEE J. Quantum Electron. **23**, 1806–1811 (1987).
5. W. Zheng, W. Lau, C. Christopher, K. C. Soo, and M. Oliva, "Optimal excitation-emission wavelengths for autofluorescence diagnosis of bladder tumors," Int. J. Cancer **104**, 477–481 (2003).
6. Y. Yang, E. J. Celmer, J. A. Koutcher, and R. R. Alfano, "UV reflectance spectroscopy probes DNA and protein changes in human breast tissues," J. Clin. Laser Med. Surg. **19**, 35–39 (2001).
7. G. M. Palmer, C. Zhu, T. M. Breslin, F. Xu, K. W. Gilchrist, and N. Ramanujam, "Comparison of multiexcitation fluorescence and diffuse reflectance spectroscopy for the diagnosis of breast cancer," IEEE Trans. Biomed. Eng. **50**, 1233–1242 (2003).
8. Y. Pu, W. Wang, G. Tang, and R. R. Alfano, "Changes of collagen and nicotinamide adenine dinucleotide in human cancerous and normal prostate tissues studies using native fluorescence spectroscopy with selective excitation wavelength," J. Biomed. Opt. **15**, 047008 (2010).
9. C. Morrison, J. Thornhill, and E. Gaffney, "The connective tissue framework in the normal prostate, BPH and prostate cancer: analysis by scanning electron microscopy after cellular digestion," Urol. Res. **28**, 304–307 (2000).
10. I. Georgakoudi, B. C. Jacobson, M. G. Muller, E. E. Sheets, K. Badizadegan, D. L. Carr-Locke, C. P. Crum, C. W. Boone, R. R. Dasari, J. Van Dam, and M. S. Feld, "NAD(P)H and collagen as in vivo quantitative fluorescent biomarkers of epithelial precancerous changes," Cancer Res. **62**, 682–687 (2002).
11. R. Richards-Kortum and E. Sevick-Muraca, "Quantitative optical spectroscopy for tissue diagnosis," Annu. Rev. Phys. Chem. **47**, 555–606 (1996).
12. D. C. G. De Veld, M. Skurichina, M. J. H. Witjes, R. P. W. Duin, H. J. C. M. Sterenborg, W. M. Star, and J. L. Roodenburg, "A clinical study for classification of benign, dysplastic, and malignant oral lesions using autofluorescence spectroscopy," J. Biomed. Opt. **9**, 940–950 (2004).
13. L. Rigacci, R. Alterini, P. A. Bernabei, P. R. Ferrini, G. Agati, F. Fusi, and M. Monici, "Multispectral imaging autofluorescence microscopy for the analysis of lymph-node tissues," Photochem. Photobiol. **71**, 737–742 (2000).
14. S. G. Demos, A. J. Vogel, and A. H. Gandjbakhche, "Advances in optical spectroscopy and imaging of breast lesions," J. Mammary Gland Biol. Neoplasia **11**, 165–181 (2006).
15. Y. Yang, E. J. Celmer, M. J. Szczepaniak, and R. R. Alfano, "Excitation spectrum of malignant and benign breast tissues: a potential optical biopsy approach," Lasers Life Sci. **7**, 249–265 (1996).
16. R. R. Alfano and Y. Yang, "Stokes shift emission spectroscopy of human tissue and key biomolecules," IEEE J. Quantum Electron. **9**, 148–153 (2003).
17. T. Vo-Dinh, "Multicomponent analysis by synchronous luminescence luminescence spectrometry," Anal. Chem. **50**, 396–401 (1978).
18. J. Ebenezar, P. Aruna, and S. Ganesan, "Synchronous fluorescence spectroscopy for the detection and characterization of cervical cancers in vitro," Photochem. Photobiol. **86**, 77–86 (2010).
19. J. Ebenezar, P. Aruna, and S. Ganesan, "Stokes shift spectroscopy for breast cancer diagnosis," Proc. SPIE **7561**, 75610B (2010).
20. V. Masilamani, D. Rabah, M. Alsalhi, V. Trinka, and P. Vijayaraghavan, "Spectra discrimination of benign and malignant prostate tissues: a preliminary report," Photochem. Photobiol. **87**, 208–214 (2011).

21. R. S. DaCosta, H. Andersson, and B. C. Wilson, "Molecular fluorescence excitation-emission matrices relevant to tissue spectroscopy," Photochem. Photobiol. **78**, 384–392 (2003).
22. B. Chance, B. Schoener, R. Oshino, F. Itshak, and Y. Nakase, "Oxidation-reduction ratio studies of mitochondria in freeze-trapped samples: NADH and flavoprotein fluorescence signals," J. Biol. Chem. **254**, 4764–4771 (1971).
23. D. C. G. De Veld, T. C. Bakker Schut, M. Skurichina, M. J. H. Witjes, J. E. Van der Wal, J. L. N. Roodenburg, and H. J. C. M. Sterenborg, "Autofluorescence and Raman microspectroscopy of tissue sections of oral lesions," Lasers Med. Sci. **19**, 203–209 (2005).
24. D. Theodorescu and T. L. Krupski, "Prostate cancer diagnosis and staging," Medscape Reference, http://emedicine.medscape.com/article/458011-overview (2009).
25. D. L. Heintzelman, R. Lotan, and R. Richards-Kortum, "Characterization of autofluorescence of polymorphonuclear leukocytes, mononuclear leukocytes and cervical epithelial cancer cells for improved spectroscopic discrimination of inflammation from dysplasia," Photochem. Photobiol. **71**, 327–332 (2000).
26. J. R. Lackowicz, *Principles of Fluorescence Spectroscopy* (Plenum, 1983).
27. D. Parmeswarn, S. Ganesan, R. Nalini, P. Aruna, V. Veeraganesh, and R. R. Alfano, "Native cellular fluorescence characteristics of normal and malignant epithelial cells from human larynx," Proc. SPIE **2979**, 759–764 (1997).
28. J. D. Pitts, R. D. Sloboda, K. H. Dragnev, E. Dmitrovsky, and M. A. Mycek, "Autofluorescence characteristics of immortalized and carcinogen-transformed human bronchial epithelial cells," J. Biomed. Opt. **6**, 31–40 (2001).
29. A. S. Ladokhin, "Fluorescence spectroscopy in peptide and protein analysis," in *Encyclopedia of Analytical Chemistry*, R. A. Meyers, ed. (Wiley, 2000), pp. 5762–5779.
30. C. Morrison, J. Thornhill, and E. Gaffney, "The connective tissue framework in the normal prostate, BPH and prostate cancer: analysis by scanning electron microscopy after cellular digestion," Urol. Res. **28**, 304–307 (2000).
31. D. F. Gleason and G. T. Mellinger, "Prediction of prognosis for prostatic adenocarcinoma by combined histological grading and clinical staging," J. Urol. **111**, 58–64 (1974).
32. R. Drezek, K. Sokolov, U. Utzinger, I. Boiko, A. Malpica, M. Follen, and R. Richards-Kortum, "Understanding the contributions of NADH and collagen to cervical tissue fluorescence spectra: modeling, measurements, and implications," J. Biomed. Opt. **6**, 385–396 (2001).
33. M. M. Sholley, G. P. Ferguson, and H. R. Seibel, "Mechanisms of neovascularization: vascular sprouting can occur without proliferation of endothelial cells," Lab. Invest. **51**, 624–634 (1984).
34. Z. Volynskaya, A. S. Haka, K. L. Bechtel, M. Fitzmaurice, R. Shenk, N. Wang, J. Nazemi, R. R. Dasari, and M. S. Feld, "Diagnosing breast cancer using diffuse reflectance spectroscopy and intrinsic fluorescence spectroscopy," J. Biomed. Opt. **13**, 024012 (2008).